Dynamics of Polymer Adsorption from Bulk Solution onto Planar Surfaces

Niklas Källrot,* Martin Dahlqvist, and Per Linse

Physical Chemistry, Center for Chemistry and Chemical Engineering, Lund University, P.O. Box 124, S-221 00 Lund, Sweden

Received January 10, 2009; Revised Manuscript Received March 9, 2009

ABSTRACT: Polymer adsorption of uncharged homopolymers onto planar surfaces has been investigated by employing a coarse-grained bead−spring polymer model using simulation techniques. Polymer solutions of two different densities and polymers of two different contour lengths have been examined. The dynamics of the adsorption process appearing in systems composed of a polymer solution placed near attractive, but initially polymer-free, surfaces were determined by Brownian dynamics simulations and equilibrium properties of corresponding systems by Monte Carlo simulations. The properties of the systems have been analyzed by monitoring the number of adsorbed polymers, bead density profiles, time and frequency of polymer attachments, spatial extension of polymers perpendicular and parallel to the surface, and configurational characteristics. Initially, the polymers diffuse toward the surfaces, and at shorter distances the attractive surface potential starts to pull the polymers toward the surface, making them slightly stretched perpendicular to the surface. Thereafter, the polymers collapse onto the surface with multiple anchoring, and a slower relaxation increasing the extension of the polymers parallel to the surfaces appears. Finally, at even longer times, and connected to the slow relaxation of the number of adsorbed polymers, the extension of the polymer coils parallel to the surface is reduced, and the perpendicular extension is increased, with associated changes of the number of beads residing in tails, loop, and trains. The adsorption process becomes faster at decreasing polymer length and at increasing polymer density.

1. Introduction

If a solid surface is exposed to a polymer solution, polymer adsorption onto the surface takes place, provided there is a sufficient attractive force between polymer segments and the surface. The attraction must exceed some threshold value to overcome the entropy loss associated with the adsorption.[1] Polymer adsorption has been studied extensively for a long time, and understanding and controlling polymer adsorption onto solid surfaces is a key issue in technical areas such as paper industry, paint formulation, and pharmacy.[2] More recently, there is a growing interest in adsorption of biopolymers such as proteins onto solid surfaces, which may reveal important information on conformation, function, and kinetics of proteins.[3,4]

The nature of polymer adsorption depends on a large number of factors, such as the properties of the solvent, polymer, and the surface. The interplay between these properties regulates the entire adsorption process, from the initial surface contact to an equilibrated polymer layer. Experimentally, there is a lot of interest in surface coverage and layer thickness,[5] which often determines the physical and mechanical properties of polymer-modified surfaces. However, it is not always clear how the dynamics of the initial adsorption process influences the final structure of the adsorbed layer. Moreover, in many cases the kinetics is a slow and sluggish and may not attain full equilibrium even after long times. There is thus also a large interest in nonequilibrium effects in adsorbed polymer layers, of which were excellently reviewed by O'Shaughnessy and Vavylonis.[6]

Because polymer adsorption is ubiquitous, with huge implications in both technology and nature, there exists a vast amount of research on this topic. Numerous approaches have been utilized in order to model and describe polymer adsorption. Characterizing equilibrium density profiles close to adsorbing surfaces has been established using mean-field approaches.[7,8] A simple theoretical kinetic model has been proposed[9] along with dynamic mean-field simulation schemes[10] to study dynamics of adsorption. Simulation methods have been used to examine static properties of adsorbed polymer layers.[11,12] The formation and growth of adsorbed layers have been studied[13−18] as well as exchange kinetics in the adsorbed layer[19,20] and detachment rates.[12,21,22] In some cases the polymers were confined between two adsorbing planes.[23] Theoretical studies and simulations have also focused on the adsorption of polyelectrolytes onto planar surfaces, with varying surface charge and charge distribution.[16,17] In most of these simulation studies on adsorption, Monte Carlo techniques have been used;[11,12,14,15,19−22] other studies were conducted employing molecular dynamics.[17,23]

The transition of a polymer from bulk to fully relaxed equilibrium structure on a solid surface is a complex process involving several stages comprising different time scales. In the previous work done by Källrot and Linse,[24] three distinct phases of the adsorption process of a single homopolymer were given: (i) an initial distortion phase, where the polymer becomes deformed by its weak interaction with the solid surface; (ii) an attachment phase, where the polymer starts to physically attach to the surface and partly spread on it; and (iii) the relaxation phase, during which the polymer continues to spread on the surface until it reaches full equilibrium. When the adsorption takes place from a polymer solution, the situation becomes more complicated due to the polymer−polymer interaction between adsorbed polymers. The effect of the polymer−polymer interaction increases during the adsorption process as more polymers are adsorbed.

In this study, we investigate mainly dynamical aspects of polymer adsorption from solution onto a planar surface. The study was conducted using a coarse-grained spring−bead polymer model, employing Brownian and Monte Carlo simulations. Two different chain lengths and two different densities have been considered. In particular, near the end of the adsorption process the repulsive polymer−polymer interaction leads to an additional shape and conformational relaxation of adsorbed polymers.

* To whom correspondence should be addressed.

10.1021/ma900050a CCC: $40.75
Published on Web 04/24/2009

2. Model

Basically, the same model is used as previously described.[24] The dynamics of polymers adsorbing from solution onto a planar surface is studied using a simple coarse-grained model. The solution contains N_p polymers, and each polymer is represented by a sequence of N_b spherical beads connected via harmonic potentials. The total number of beads in the system N is thus given by $N = N_p N_b$. The polymers are confined in a rectangular simulation box with the box lengths L_x, L_y, and L_z. At $z = \pm(L_z/2)$ we have adsorbing surfaces, whereas periodic boundary conditions are applied in the x- and y-directions. The length of the box edges are $L_x = L_y = 200$ Å and $L_z = 240$ Å.

Because the two surfaces are equivalent, we will average our results over both of them. Furthermore, since we will focus on events occurring near the surfaces, we will in the following adopt a coordinate system, in which the z-axis starts at $z = L_z/2$ with its direction pointing into the solution.

The total potential energy U for the system can be expressed as a sum of three different terms (nonbonded bead−bead potential energy $U_{nonbond}$, bond potential energy U_{bond}, and a bead−surface potential energy U_{surf}) according to

$$U = U_{nonbond} + U_{bond} + U_{surf} \quad (1)$$

The nonbonded bead−bead potential energy is assumed to be pairwise additive according to

$$U_{nonbond} = \sum_{i<j}^{N} u(r_{ij}) \quad (2)$$

where the truncated and shifted repulsive Lennard-Jones (LJ) potential energy

$$u(r_{ij}) = \begin{cases} 4\varepsilon\left[-\left(\frac{\sigma}{r_{ij}}\right)^6 + \left(\frac{\sigma}{r_{ij}}\right)^{12} + \frac{1}{4}\right], & r_{ij} \le 2^{1/6}\sigma \\ 0, & r_{ij} > 2^{1/6}\sigma \end{cases} \quad (3)$$

is used for the interaction between beads i and j, with r_{ij} being the distance between the two beads, $\sigma = 3.405$ Å the diameter of the bead, and $\varepsilon = 0.9961$ kJ/mol the interaction strength. The truncation and the shift of the Lennard-Jones potential yield a soft repulsive potential.

The bond potential energy is given by

$$U_{bond} = \frac{1}{2}k_{bond}\sum_{i=1}^{N_p(N_b-1)}(r_i - r_{eq})^2 \quad (4)$$

where $k_{bond} = 2.4088$ kJ/mol is the bond force constant and $r_{eq} = 5.0$ Å the equilibrium bond length. The model does not include any intrinsic stiffness of the chains, and therefore all chains are considered as fully flexible. In the presence of all interactions, the root-mean-square (rms) bead−bead separation of bonded beads along the chains becomes $\langle R_{bb}^2\rangle^{1/2} \approx 5.6$ Å.

The polymer−surface interaction is taken as a sum of bead−surface interactions according to

$$U_{surf} = \sum_{i=1}^{N} u_{surf}(z_i) + u_{surf}(L_z - z_i) \quad (5)$$

where an attractive 3−9 LJ potential[25]

$$u_{surf}(z_i) = \frac{2\pi}{3}\rho_s{\sigma_s}^3\varepsilon_s\left[-\left(\frac{\sigma_s}{z_i}\right)^3 + \frac{2}{15}\left(\frac{\sigma_s}{z_i}\right)^9\right] \quad (6)$$

is used for the interaction between bead i and the surface in the adsorption simulations. In eq 6, ρ_s is the density of the (hypothetical) particles forming the surface, σ_s the mean diameter of beads and surface particles, ε_s a potential energy parameter describing the bead−surface interaction, and z_i the z-coordinate of bead i with respect to (the nearest) surface. For simplicity, $\sigma_s = 3.5$ Å and $\rho_s{\sigma_s}^3 = 1$ were chosen. With this attractive 3−9 LJ potential, the potential minimum appears at $z_{min} = (2/5)^{1/6}\sigma_s \approx 3.0$ Å and amounts to $u_{surf}(z_{min}) = -[2\pi(10)^{1/2}/9]\rho_s{\sigma_s}^3\varepsilon_s \approx -2.2\varepsilon_s$. Model parameters are compiled in Table 1.

Table 1. Model Parameters

box length (x, y-dir)	$L_x = L_y = 200$ Å
box length (z-dir)	$L_z = 240$ Å
temperature	$T = 298$ K
number of beads in a chain	$N_b = 20$ and 80
bead−bead LJ parameter	$\sigma = 3.405$ Å
bead−bead LJ parameter	$\varepsilon = 0.9961$ kJ/mol
force constant of bond potential	$k_{bond} = 2.4088$ kJ/mol
equilibrium separation of bond potential	$r_{eq} = 5.0$ Å
bead−surface LJ parameter	$\sigma_s = 3.5$ Å
bead−surface LJ parameter	$\varepsilon_s = 2.5$ kJ/mol

Table 2. Specifications of Investigated Systems

label	N_b	N_p	ϕ_b[a]	c/c^*[b]
ld20	20	268	0.0115	0.23
hd20	20	1056	0.0455	0.90
hd80	80	83	0.0143	0.90

[a] Bead volume fraction. [b] The overlap density c^* was estimated using the radius of gyration at infinite dilution.

In this work, polymers with chain lengths $N_b = 20$ and 80 have been considered. Two systems with $N_b = 20$ at densities equivalent to ≈20 and ≈90% of its overlap density, were studied. A third system with $N_b = 80$ has also been investigated at the higher of these two densities. The lower density corresponds to a solution in the dilute regime, and the higher one is located on the border between the dilute and the semidilute regime. Table 2 provides data of the three polymer solutions.

3. Method

In this work, both static and dynamic properties of polymer solutions have been examined. Brownian dynamics (BD) simulations were used to examine the adsorption dynamics and the associated change of the internal structure of the polymers, whereas Monte Carlo (MC) simulations were used to obtain equilibrium properties. MC simulations were also used to prepare the initial configurations of the BD simulations.

In more detail, the adsorption simulation studies were carried out as follows: (i) First, an equilibrated polymer solution was generated by MC simulations using a slightly smaller box to generate polymer-free zones adjacent to the adsorbing surfaces in the subsequent BD simulations. Here, we used $L_z = 200$ Å with hard walls at the edges in the z-directions. (ii) Second, the hard walls were removed, the box length in the z-direction was increased to $L_z = 240$ Å, and attractive surfaces, whose potential was described by eq 6, were invoked. (iii) The BD simulations were performed. Hence, the initial configurations of the BD simulations involved a ≈20 Å thick polymer-free zone adjacent to each surface.

In complement to the adsorption simulation, BD and MC simulations of corresponding bulk systems were performed to provide properties of the bulk solutions. These simulations were performed with periodic boundary conditions applied in all three directions. Naturally, in these simulations the U_{surf} term in eq 1 was absent.

The motion of the polymer beads in the BD simulations was described by Ermak[26]

$$\mathbf{r}_i(t + \Delta t) = \mathbf{r}_i(t) + \frac{D_0\Delta t}{k_b T}\mathbf{F}_i(t) + \mathbf{R}_i(t;\Delta t) \quad (7)$$

where $\mathbf{r}_i(t + \Delta t)$ is the location of bead i at the time $t + \Delta t$, $\mathbf{r}_i(t)$ the location of bead i at the time t, D_0 the bead self-diffusion

coefficient in the absence of systematic forces, k_b Boltzmann's constant, T the temperature, and $F_i(t)$ the systematic force on bead i at time t arising from the potential energy U given by eq 1. Furthermore, $\mathbf{R}_i(t;\Delta t)$ is a random displacement of bead i representing the effect of collisions with solvent molecules at time t and is sampled from a Gaussian distribution with the mean $\langle \mathbf{R}_i(t;\Delta t)\rangle = 0$ and the variance $\langle \mathbf{R}_i(t;\Delta t)\cdot\mathbf{R}_j(t';\Delta t)\rangle = 6D_0\Delta t\delta_{ij}\delta(t-t')$ as obtained from the fluctuation−dissipation theorem. In this work, hydrodynamic interactions were neglected.

A bead self-diffusion coefficient $D_0 = 0.1$ Å^2/ps was used, and an integration time step $\Delta t = 0.025$ ps was employed. The BD simulations involved 4×10^7 time steps, providing a nominal simulation time of 1 μs. Using $\tau_{BD} = \sigma^2/D_0 = 116$ ps as the conventional unit of time, the integration time step becomes $\Delta t = 2.2 \times 10^{-4}\tau_{BD}$ and the total simulation time $8.6 \times 10^3\tau_{BD}$.

The MC simulations were performed according to the Metropolis algorithm,[27] using three types of trial moves: (i) translation of individual beads, (ii) reptation of polymers, and (iii) translation of entire polymers. The translational displacement parameter of single-bead trial moves was 3 Å, the probability of a reptation and of a chain translation was $1/N_b$ of that of a single-bead trial move, and the chain translational displacement parameter was 5 Å. The MC simulations comprised 2×10^5 trial moves per bead after equilibration. All simulations were performed using the integrated Monte Carlo/molecular dynamics/Browninan dynamics simulation package MOLSIM.[28]

4. Dynamical Analysis

Several time-dependent properties were examined during the adsorption process of the chains. The location of a polymer at a time t was described using its center of mass $r_{com}(t)$ defined according to

$$\mathbf{r}_{com}(t) = \frac{1}{N_b}\sum_{i=1}^{N_b}\mathbf{r}_i(t) \tag{8}$$

where $\mathbf{r}_i(t) = [x_i(t), y_i(t), z_i(t)]$ is the coordinate of bead i at time t. Changing the notation $\mathbf{r}_i(t)$ to $z_i(t)$ in eq 8 gives the center of mass along the z-axis, $z_{com}(t)$, which is a useful measure of the position of the polymers relative to a surface.

The extension of the polymers in three dimensions at time t is given by its rms radius of gyration, $\langle R_g^2(t)\rangle^{1/2}$, defined according to

$$\langle R_g^2(t)\rangle = \left\langle \frac{1}{N_b}\sum_{i=1}^{N_b}[\mathbf{r}_i(t) - \mathbf{r}_{com}(t)]^2 \right\rangle \tag{9}$$

There is a structural rearrangement of the polymers from essentially a 3- to 2-dimensional object during the adsorption. This deformation of a polymer was followed by studying the perpendicular ($\perp$) and parallel ($\|$) component of $\langle R_g^2(t)\rangle^{1/2}$ according to

$$\langle R_g^2(t)\rangle_\perp = \left\langle \frac{1}{N_b}\sum_{i=1}^{N_b}[z_i(t) - z_{com}(t)]^2 \right\rangle \tag{10}$$

$$\langle R_g^2(t)\rangle_\| = \left\langle \frac{1}{N_b}\sum_{i=1}^{N_b}\{[x_i(t) - x_{com}(t)]^2 + [y_i(t) - y_{com}(t)]^2\} \right\rangle \tag{11}$$

satisfying $\langle R_g^2(t)\rangle = \langle R_g^2(t)\rangle_\perp + \langle R_g^2(t)\rangle_\|$.

A polymer was considered as being adsorbed if at least one of its beads was in contact with a surface, here defined by $z_i <$ 6 Å. Recall that the minimum of the bead−surface potential is located at $z_{min} \approx 3$ Å. The criteria for when a polymer is considered adsorbed is somewhat arbitrary. The choice of adsorption distance will generally influence the numbers obtained but not qualitative aspects.

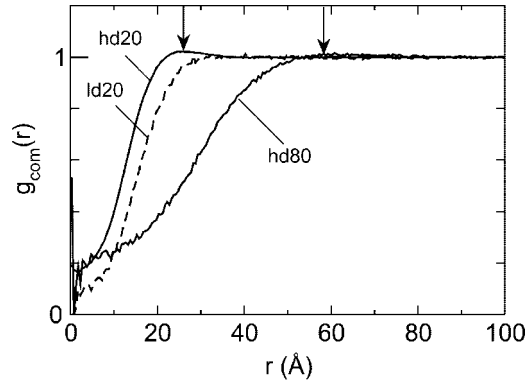

Figure 1. Center-of-mass radial distribution function $g_{com}(r)$ of indicated bulk systems. The mean diameters of the polymer coils at indicated number of monomers at infinite dilution are shown by arrows.

The structure of adsorbed polymers was described by using loop, tail, and train subchains.[5] A subchain of adsorbed beads is referred to as a train, a nonadsorbed subchain with both ends bonded to trains as a loop, and a nonadsorbed subchain with one end bonded to a train as a tail. The average total number of beads in subchains of type α at time t will be denoted by $\langle N_\alpha(t)\rangle$, with $\alpha = \{\text{loop, tail, train}\}$. By conservation, $\sum_\alpha\langle N_\alpha(t)\rangle = N_b$.

The relaxation of properties from their initial values to their equilibrium values were also examined. That was performed by monitoring

$$q(t) = \frac{\langle X(t)\rangle - X_{eq}}{\langle X(0)\rangle - X_{eq}} \tag{12}$$

where $X(t)$ denotes the value of the property X at time t, $X(0)$ its initial value at time $t = 0$, and X_{eq} its equilibrium value. Relaxation times were extracted by single or biexponential fits of $\ln q(t)$ vs t.

The brackets $\langle ... \rangle$ in eqs 9−12 and elsewhere depend on boundary conditions and simulation method. In the MC simulations, they normally denote an ensemble and polymer average, whereas in the BD simulation of bulk systems they represent a time and polymer average, and finally in the nonequilibrium BD simulations of the surface systems they denote an average over adsorbed polymers.

5. Bulk Solution

The bulk solutions containing polymers of the different polymer lengths and densities were characterized using data obtained from both BD and MC simulations. Table 3 provides some key data and Figure 1 the center-of-mass radial distribution function $g_{com}(r)$ of the three systems investigated.

Table 3. Properties of Investigated Bulk Systems

label	$\langle R_g^2\rangle^{1/2}$ (Å)	D (Å^2/ns)[a]	τ_R (ns)[b]
20[c]	12.50 ± 0.01	5 ± 1	9 ± 3
ld20	12.35 ± 0.05	5 ± 1	9 ± 3
hd20	11.90 ± 0.05	4 ± 1	8 ± 3
80[c]	29.2 ± 0.1	0.9 ± 0.2	$2 \times 10^2 \pm 100$
hd80	27.9 ± 0.3	0.8 ± 0.2	100 ± 50

[a] The polymer self-diffusion coefficient D was obtained from a linear least-squares fit of the mean-square displacement as a function of time. [b] The end-to-end vector correlation time τ_R was obtained from a biexponential fit, using the slowest decaying term with a relative amplitude >90%. [c] At infinite dilution.

Our earlier simulations[24] of the polymer model used showed that the radius of gyration at infinite dilution scales as $\langle R_g^2\rangle^{1/2} \sim N_b^{\nu}$ with $\nu \approx 0.59 \pm 0.1$, in agreement with the theoretical prediction $\nu = 0.588$ for chains in a good solvent.[29] Table 3 shows that the radius of gyration decreases marginally at the finite densities considered. The reduction amounts to less than ≈5% as compared to a polymer solution at infinite dilution. This modest effect is understood from the fact that at the highest density considered the overlap condition is about to be reached.

Figure 1 shows that $g_{com}(r) < 1$ at short separation, implying that polymer coils are repelling each other. However, $g_{com}(r) > 0$, even at $r = 0$, demonstrating interpenetrating coils. At large separation, typically starting at $r \approx 2\langle R_g^2\rangle^{1/2}$, we have $g_{com}(r) = 1$, implying that spacial correlations are lost at these distances. In more detail, at the higher density of the $N_b = 20$ system the value of $g_{com}(0)$ is larger and the rise of the radial distribution function appears at shorter separation, demonstrating a larger degree of interpenetration. Furthermore, a small but significant maximum appears at $r \approx 2(R_g^2)^{1/2}$, indicating a weak ordering of nearest-neighbor polymer coils.

Data of the diffusion coefficient D are given in Table 3. At infinite dilution, D is consistent with $D = D_0/N_b$ as predicted for Rouse dynamics of isolated chains. At the finite densities considered here, D decreases at most 10% at the lower and 10−20% at the higher density; however, these changes are within the statistical uncertainties.

The end-to-end vector autocorrelation function was examined to study the internal relaxation of the chains. These functions displayed a biexponential behavior, where the fastest mode involved at most 10% of the amplitude. The relaxation times τ_R of the second slower mode for the different systems are also given in Table 3. At infinite dilution it was found that $\tau_R \sim N^{\alpha}$ with $\alpha \approx 2.5$.[24] The theoretical estimation of the exponent for a single polymer in a good solvent with Rouse dynamics is $\alpha = 1 + 2\nu$, with $\nu = 0.588$. The fitted τ_R are subjected to substantial uncertainties, and as for the self-diffusion coefficient, no significant density dependence of τ_R was found.

6. Adsorption

We will now continue with the results from the adsorption investigation with a focus on the results from the BD simulations. The section is organized as follows: (i) first, general features of the polymer adsorption are briefly discussed, and (ii) thereafter, we more thoroughly describe the influence of polymer density and polymer length on the adsorption process.

6.1. General Features. As previously mentioned, the polymer solutions were equilibrated in a cubic box, whose length in the z-direction was extended at each side by 20 Å before the BD simulations were started with the adsorbing surfaces present. Therefore, at the start ($t = 0$) of the BD simulations, a ≈20 Å thick polymer-free zone adjacent to each surface was present. Next to this zone there was a gradual increase of the bead density in a slab of a thickness of about a radius of gyration before the bead density leveled off. This gradual increase is due to a depletion occurring in the vicinity of the hard walls in the equilibration simulations. Beads located 20 Å from a surface experience the negligible potential $u_{surf} = 1.1 \times 10^{-3}\, k_bT$, which is only 0.05% of the value at z_{min}.

During the initial part of the BD simulations the polymers diffuse toward a surface through collective diffusion. First at a later stage, the surface potential becomes effective, and the attractive surface force accelerates the motion of beads toward a surface. The beads of a polymer coil, which faces a surface are those first affected, resulting in an elongation of the polymer coil in the z-direction.[24] These beads become subsequently attached to the surface and start to spread on it. Other beads of the polymer coil not yet attracted by the surface are thereby "pulled" toward the surface through the chain connectivity, described as a "zipping" mechanism.[30] At this stage, the extension of the polymer coil perpendicular to the surface is reduced, and the spread of the coil on the surface increases its extension in the in-plane direction. As will be shown, at an even later stage of the adsorption the conformations of adsorbed polymers are changed.

Table 4. Equilibrium Properties of Adsorbed Polymers of Investigated Systems

	$\langle N_p^{ads}\rangle^a$	$\langle N_b^{ads}\rangle^b$	$\langle R_g^2\rangle_{\perp}^{1/2}$ (Å)^d	$\langle R_g^2\rangle_{\parallel}^{1/2}$ (Å)^d	$\langle R_g^2\rangle^{1/2}$ (Å)^d
20[c]	1	12.7 ± 0.1	2.9	13.0	13.3
ld20	147.5 ± 0.8	1465 ± 9	4.6	10.9	11.8
hd20	246.7 ± 0.8	2001 ± 5	5.5	10.2	11.6
80[c]	1	52.9 ± 0.1	2.8	34.9	35.1
hd80	54.4 ± 0.5	1725 ± 9	10.2	24.2	26.3

[a] Number of adsorbed polymers at the two surfaces. [b] Number of adsorbed beads at the two surfaces. [c] At infinite dilution. [d] Largest estimated uncertainty for the rms radius of gyration is 5%.

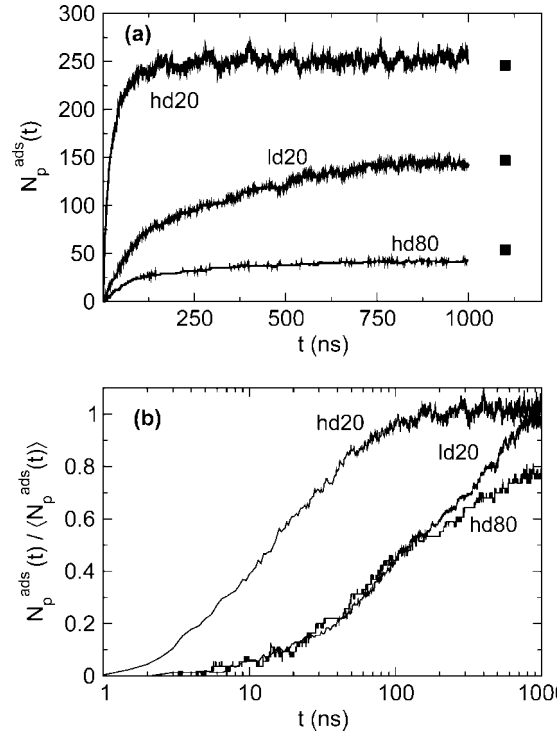

Figure 2. (a) Number of adsorbed polymers $N_p^{ads}(t)$ and (b) normalized number of adsorbed polymers as a function of time t for indicated systems. In (a), $\langle N_p^{ads}\rangle$ at equilibrium from MC simulations (filled squares) are also given.

6.2. Variation of Polymer Density and Length.

6.2.1. Number of Adsorbed Polymers. A central feature of the adsorption process is the number of adsorbed polymers. Table 4 provides the equilibrium number of adsorbed polymers at the two surfaces $\langle N_p^{ads}\rangle$ obtained from the MC simulations. First, we notice that $\langle N_p^{ads}\rangle$ is ≈30% higher for the hd20 system as compared to the ld20 system. Furthermore, in the ld20 system ≈2/3 and in the hd20 system ≈1/4 of the polymers are adsorbed (cf. data in Tables 2 and 4). This implies that the polymer densities far from the surfaces are reduced by the factors 3 and 1.25, respectively, as compared to the stoichiometric ones given in Table 2. This is of course important when relating adsorbed amount to bulk densities or activities but is of less concern for our (general) characterization of the adsorption dynamics.

Figure 2 displays the number of adsorbed polymers $N_p^{ads}(t)$ as a function of the time t of the three systems. Subplot a shows $N_p^{ads}(t)$ on a linear time scale and the equilibrium values $\langle N_p^{ads}\rangle$,

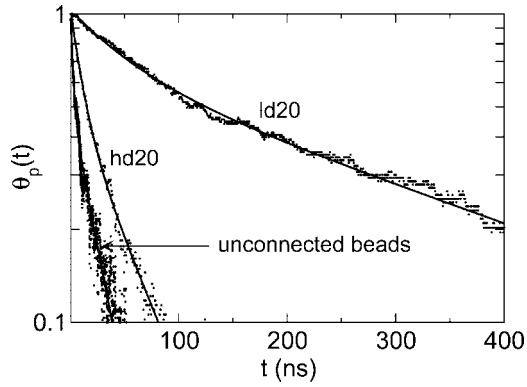

Figure 3. Relaxation of the adsorbed amount of polymers and unconnected beads at the attractive surface $\theta_p(t)$ to their equilibrium values as a function of time t (dots) and biexponential fits (solid lines) for indicated systems.

whereas subplot b gives the number of adsorbed polymers normalized by their equilibrium values presented on a logarithmic time scale. The upper t-limit marks the end of the BD simulation. Here in subplot b, and in other figures, data are given on a logarithmic time scale to encompass processes occurring at widely different time scales. The hd20 system attains the equilibrium amount of adsorbed polymers at $t \approx 200$ ns. Regarding the ld20 and hd80 systems, at the lower density (ld20 system) and the hd80 system, we find that the equilibrium amount of adsorbed polymers is not achieved even after 1000 ns; however, it is relatively close to it in both systems.

The rate at which the number of adsorbed polymers relaxes toward its equilibrium value have been investigated in further detail. From $N_p^{ads}(t)$ the associated relaxation function $\theta_p(t)$ given by eq 12 was formed. Figure 3 shows $\theta_p(t)$ and biexponential fits for the ld20 and hd20 systems and a system composed of unconnected beads at $\phi_b = 0.0115$, which was prepared in the same way as the polymer systems. The time constants for the biexponential fits were 0.0029 and 0.018 ns^{-1} for the ld20 system and 0.020 and 0.094 ns^{-1} for the hd20 system. In both systems, the amplitudes of the two modes appear to be roughly the same. The similar appearance of a biexponential decay for the system with unconnected beads suggests that this appearance is not related to polymers. A tentative explanation is that the first relaxation mode is associated with the adsorption onto a bare surface, whereas the second and slower mode to the adsorption onto a surface that is partly covered by beads. The rate of the faster mode for the high-density system is ≈10 times higher than for the low-density system. A comparison between the unconnected-bead system and the ld20 system shows that the polymeric nature slows down the adsorption rate 20-fold.

6.2.2. Density Profiles. The adsorption of polymers onto the surfaces leads to an enhanced bead density near the surfaces. Figure 4 displays bead density profiles $\rho_b(z)$ near a surface from the last 10th (i.e., $t = 900-1000$ ns) of the BD simulation and equilibrium density profiles from the MC simulations. Generally, a pronounced density maximum is observed at $z \approx 2.5$ Å and a weak one at $z \approx 5$ Å. Regarding the ld20 system, a complete agreement of the bead densities are found at the first maximum, whereas at further distance from the surface the bead density from the BD simulation falls slightly below that of the equilibrium one (Figure 4a). As for the hd20 system, a complete agreement is found between the BD and MC data (Figure 4b), consistent with that $N_p^{ads}(t)$ is equilibrated after $t \approx 200$ ns. In the hd80 system (Figure 4c), the densities coincide at the first and second peak, but at distances further away than 10 Å from the surface, the BD simulation result drop below the equilibrium MC results.

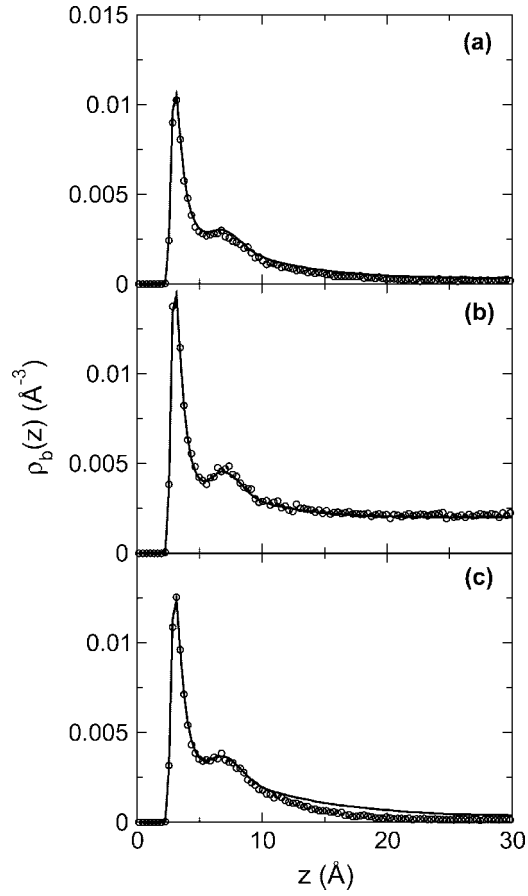

Figure 4. Bead density $\rho_b(z)$ as a function of z-coordinate near a surface for the (a) ld20, (b) hd20, and (c) hd80 systems obtained from the end ($t = 900-1000$ ns) of BD simulations (open circles) and MC simulations (solid curves).

Figure 5 shows the bead density as a function of the z-position and time near a surface. At the lower t-limit, $t = 0.1$ ns, a 20-mer at infinite dilution would have diffused 1 Å. Thus, the bead density profile at $t = 0.1$ ns is close to the initial one of the BD simulation. The general features are that (i) the spatial extension of the initially bead-free solution near the surface decreases with increasing time, (ii) thereafter a layer of beads adjacent to the surface is formed with a bead density (much) larger than the solution density, and (iii) finally a second layer of beads outside the first one is formed with a bead density smaller than that of the first layer.

As to the ld20 system (Figure 5a), beads starts to become adsorbed at $t \approx 2$ ns, and the amount of adsorbed beads increases throughout the simulation. Regarding the denser hd20 system (Figure 5b), the initial attachment of beads to the surface appears at $t \approx 1$ ns, the increase of adsorbed beads is much more rapid, and the equilibrium amount of adsorbed beads is reached at $t \approx 200$ ns. The equilibrium bead densities in both the first and second layers are larger as compared to those of the ld20 system. The smaller time for the initial adsorption in the hd20 system displayed here as well as in Figures 2 and 3 could qualitatively be understood from the faster collective diffusion in the denser system. Increasing the chain length at the higher density (Figure 5c) gives rise to a probability density profile, which displays much of the characteristics of the ld20 system. However, there is a pronounced delay in the attachment of polymers at the surface, which is partly attributed to the 4-fold smaller diffusion coefficient at infinite dilution for the longer polymer (Table 3).

Thus, both the number of adsorbed polymers and the bead density show that the hd20 system achieves equilibrium at $t \approx$

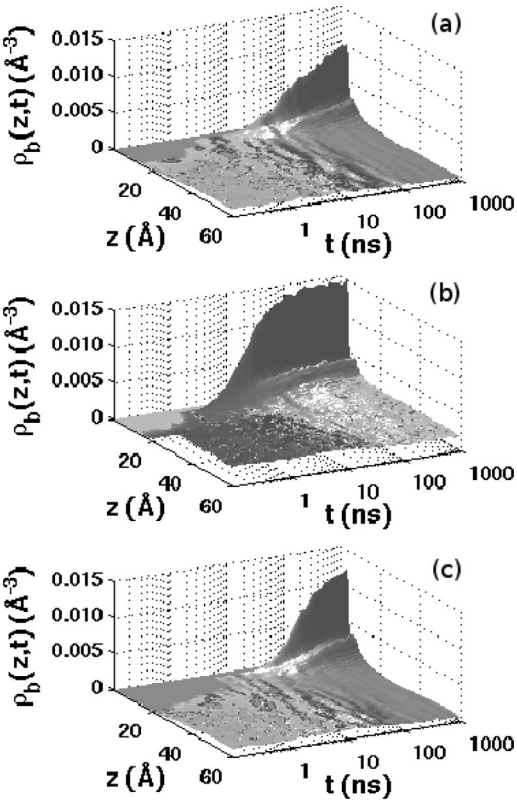

Figure 5. Bead density $\rho_b(z,t)$ as a function of z-coordinate and time t for the (a) ld20, (b) hd20, and (c) hd80 systems.

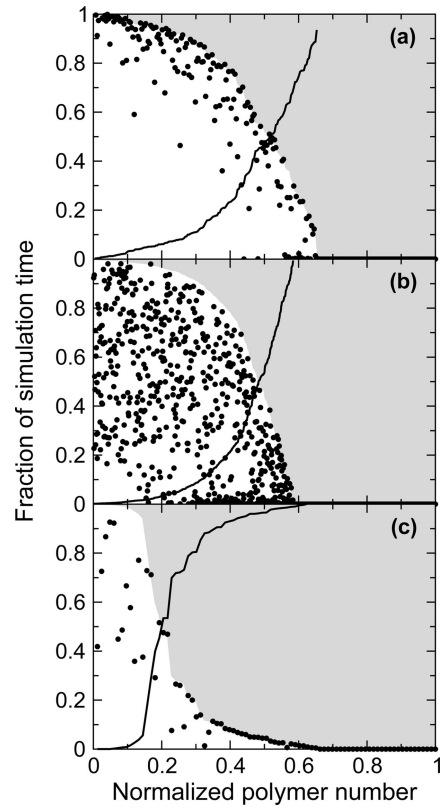

Figure 6. Fraction of simulation length as a function of normalized polymer number for the (a) ld20, (b) hd20, and (c) hd80 systems. The solid lines represent the time when a polymer was initially adsorbed, and the corresponding filled circle gives the total adsorbed time for that polymer. The border toward the shaded region represents the maximum possible adsorption time for each respective polymer.

200 ns, whereas both the ld20 and hd80 systems are close but have not yet reached equilibrium at the end ($t = 1000$ ns) of the BD simulation. The larger bead density in the hd20 system leads to an initially quicker adsorption due to a faster collective diffusion and to a larger adsorbed amount at equilibrium.

6.2.3. Rate and Frequency of Attachment and Detachment. We will now focus on the adsorption of individual polymers. In particular, we are interested in (i) the total time a single polymer is adsorbed and (ii) how that depends on whether it is adsorbed at an early or a late stage. For that purpose, we have tagged all polymers when being adsorbed. If a polymer desorbs, it loses its tag but becomes tagged again if it readsorbs.

Let us now order the polymers by the time at which they became attached to a surface for the first time. Figure 6 (solid curves) displays the fraction of the simulation time at which a polymer was adsorbed for the first time as a function of the normalized polymer number. By construction this function is an increasing function: it starts with the time at which the first polymer became adsorbed (near the start of the simulation) and ends at the time when the last polymer was adsorbed (near the end of the simulation). In Figure 6 for each polymer a dot marks the total fractional simulation time it has been adsorbed (the total time it has been being tagged divided by the simulation time). The shaded area represents the area unavailable to this property. In other words, polymers that become adsorbed the fraction x of the total simulation time can be adsorbed at most the fraction $1 - x$ of the simulation. For polymers not at all being adsorbed, $x = 1$, and hence the shaded area makes contact with the abscissa for these polymers.

The subplots a and b of Figure 6 show that 65% and 60% of the polymers in the ld20 and hd20 systems, respectively, adsorb onto a surface at some stage during the simulation. In the ld20 system, most dots appear near the boundary of the shaded region, demonstrating that a polymer that becomes adsorbed stays adsorbed for most of the remaining part of the simulation. On the contrary, in the hd20 system, there is virtually no correlation between the time for the first attachment and the total time being adsorbed. Hence, for the ld20 system the exchange of adsorbed and nonadsorbed polymers is low, which, at least partly, could be understood from the fact that the simulation comprises an equilibration process, whereas for the hd20 system ≈80% of the simulation time comprises a system at equilibrium with a dynamic exchange of polymers, involving frequent detachments of polymers. At the higher density of the longer polymer hd80, Figure 6c displays that in this system ≈65% of the polymers adsorb to the surface at some stage of the simulation. Also here, polymers that adsorb early in the simulation do not necessarily stay adsorbed for the remainder of the simulation; thus, there is quite a large degree of dynamic exchange present.

To investigate this situation further, Figure 7 displays the number of attachment occurrences of a given polymer onto a surface as a function of the normalized polymer number. Once again, the polymers are ordered in increasing time at which they attach to a surface for the first time. For both the ld20 and hd20 systems there is a large spread in the number of attachment occurrences. In the ld20 systems this property varies between 1 and 27, while for the hd20 system the variation is much larger, between 1 and 64. This concurs with the predictions of Zajac et al.,[14] who reported the motion of the polymers at the surface as a fluttering state with numerous reattachments of polymers to the surface, albeit that the values are largely governed by the precise adsorption criterion. For the ld20 and hd20 systems, the first few polymers being adsorbed display a smaller attachment occurrence; hence, they appear to be stronger adsorbed. The attachment occurrence decays at large normalized polymer number; an obvious explanation is that since these

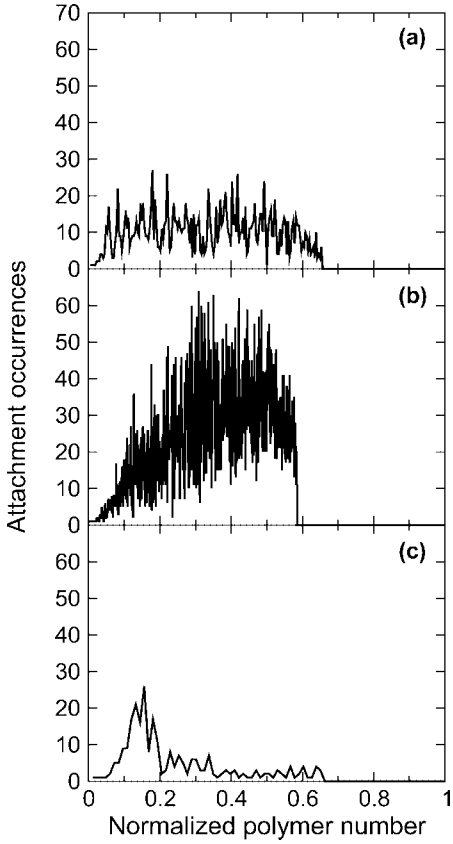

Figure 7. Attachment occurrences as a function of the normalized polymer number for the (a) ld20, (b) hd20, and (c) hd80 systems.

polymers adsorb onto the surface at a later stage of the simulation and hence less time is available for the adsorption−desorption process. For the longer polymer, hd80, the initial appearance is quite the opposite from that of the shorter polymer. The largest number of reattachments occur for the first 30% of polymers that adsorb to the surface; here we have between 5 and 26 attachment occurrences. For polymers that adsorb during the second half of the simulation, this number is reduced to rarely exceeding 5.

6.2.4. Shape and Conformational Characteristics. The rms radius of gyration and its components perpendicular and parallel to the surface of adsorbed polymers have been analyzed. Figure 8 presents the probability distribution of these quantities as a function of time as intensity plots. A distribution is normalized such that its vertical integral is proportional to the number of adsorbed polymers $N_p^{ads}(t)$ given in Figure 2a. This makes the integrated intensity to increase with increasing time and to be different among the various systems.

Subplots a, d, and g of Figure 8 provide the evolution of the radius of gyration perpendicular to the surface. Regarding the ld20 system, $P(R_g(t)_\perp)$ displays a marked increase in $R_g(t)_\perp$ during $t = 2-10$ ns, implying an elongation of the few polymers adsorbed in this time range. The presence of adsorbed polymers being elongated perpendicular to the surface appears also at a later time; however, the fraction of adsorbed polymers with such elongation decreases with time. The probability for $R_g(t)_\perp \approx 4$ Å starts to become considerable at $t \approx 30$ ns, demonstrating that adsorbed polymers start to reduce their extension in the z-direction. At $t > 70$ ns, polymers with $R_g(t)_\perp \approx 4$ Å dominates the distribution. As for the hd20 system, the general features of $P(R_g(t)_\perp)$ is similar to those of the ld20 system. However, it can be inferred that the elongation appears earlier, in the time interval 1−3 ns, consistent with the more rapid collective diffusion. During $t = 20-30$ ns most adsorbed polymers are compressed to ≈4 Å, as for the ld20 system. However, later the probability for adsorbed chains to attain larger values of $R_g(t)_\perp$ increases for the hd20 system; typically, $R_g(t)_\perp = 4-8$ Å. The equilibrium rms averages given in Table 4, $(R_g^2)_\perp^{1/2} =$ 4.6 and 5.5 Å for the ld20 and hd20 systems, respectively, confirm the larger perpendicular extension appearing in the high-density system for the shorter polymer. For the hd80 system, $P(R_g(t)_\perp)$ clearly shows an initial perpendicular extension up to 40 Å of polymers pulled by the surface attraction, and the following collapse to a few angstroms. The extension of polymers occurs later in time (≈ 5−50 ns), and the collapse is also delayed due to the initially larger radius of the polymer in solution.

The corresponding data for the parallel component of the radius of gyration are given in subplots b, e, and h of Figure 8. The time dependence of $P(R_g(t)_\parallel)$ is also similar for the ld20 and hd20 systems. In particular, at short and intermediate times $R_g(t)_\parallel$ increases, whereas at long times it slightly decreases. The maximum appears at $t \approx 100$ ns for the ld20 system and at $t \approx$ 50 ns for the hd20 system. At these and longer times, the distribution of $R_g(t)_\parallel$ toward larger values is more limited for the hd20 system. Thus, we observe initially an expansion of the polymer coils parallel to the surface, whereas for longer times a weak contraction occurs. For the hd20 system, the probability for an extended in-plane configuration is reduced as compared to the ld20 system. The rms averages $(R_g^2)_\parallel^{1/2} =$ 10.9 and 10.2 Å for the ld20 and hd20 systems, respectively, given in Table 4 confirm this. The parallel component of the radius of gyration for the hd80 system displays a quite broad distribution throughout, with a broadening of the property at ≈100 ns, which manifests the in-plane extension and the subsequent contraction of adsorbed polymers.

Subplots c, f, and i of Figure 8 show the time dependence of the distributions of the radius of gyration of the adsorbed polymers. Generally, time dependence is smaller since the time dependencies of the perpendicular and parallel components partly cancel each other.

Conformational characterization of adsorbed polymers in terms of tails, loops, and trains have been performed. Figure 9 displays the average fraction of beads residing in tails (Figure 9a), loops (Figure 9b), and trains (Figure 9c) as a function of time for the ld20 and hd20 systems. Since we are examining nonequilibrium systems, averages at a given time are generally made over different numbers of adsorbed polymers that in turn are at different of stages of their adsorption processes. Because of the variation of $N_p^{ads}(t)$ and the logarithmic time scale, the uncertainties are relatively large at small t and negligible at large t. The equilibrium values obtained from MC simulations (squares) and the equilibrium values of a single adsorbed polymer (circles) are also presented.

Figure 9 shows that initially nearly all beads of adsorbed polymers are involved in tails and the fraction of beads in loops and trains is low. Thereafter, (i) the fraction of beads in tails reduces, passes through a minimum, and finally reaches its equilibrium value, (ii) the fraction of beads in loops increases, displays a weak maximum, and finally decreases somewhat before attaining its equilibrium value, and (iii) the fraction of beads in trains grows with time, exhibits a maximum, and then displays a weak decay before the equilibrium value is attained. The initial relaxation of the ld20 system starts at a later time as compared to the hd20 system, which we relate to the slower diffusion of the polymers to a surface in the ld20 system.

The extreme values of the ld20 system appears at $t \approx$ 200−300 ns, and the values at $t = 1000$ ns almost agree with those from the equilibrium simulations (open squares), again supporting the notion that this system is close to equilibrium at the end of the BD simulation. On the other hand, the extreme

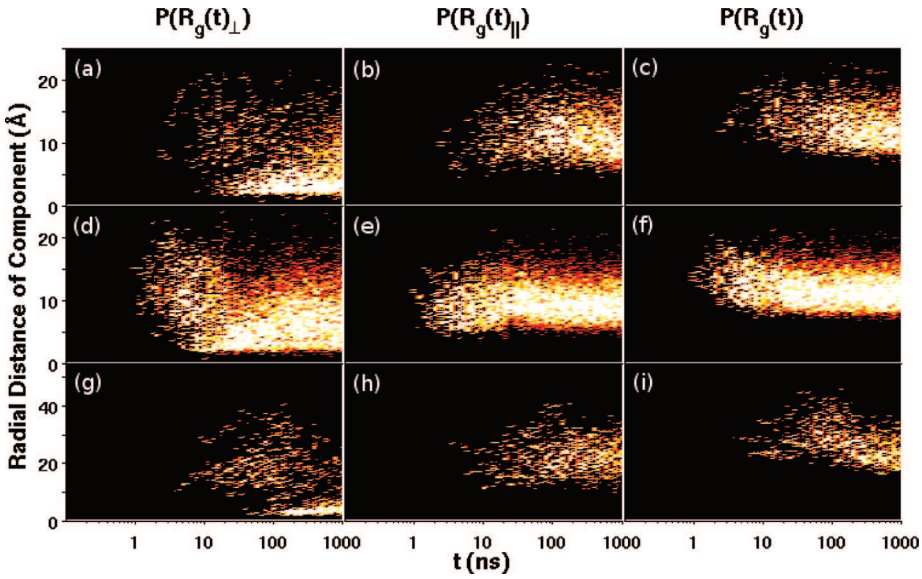

Figure 8. Probability distribution of the (left column) perpendicular component of the radius of gyration $P(R_g(t)_\perp)$, (central column) parallel component of the radius of gyration $P(R_g(t)_\parallel)$, and (right column) radius of gyration $P(R_g(t))$ of adsorbed polymers as a function of time t for the (a−c) ld20, (d−f) hd20, and (g−i) hd80 systems. Bright intensity signifies a larger probability. The vertical integral of a probability distribution at time t is proportional to $N_p^{ads}(t)$.

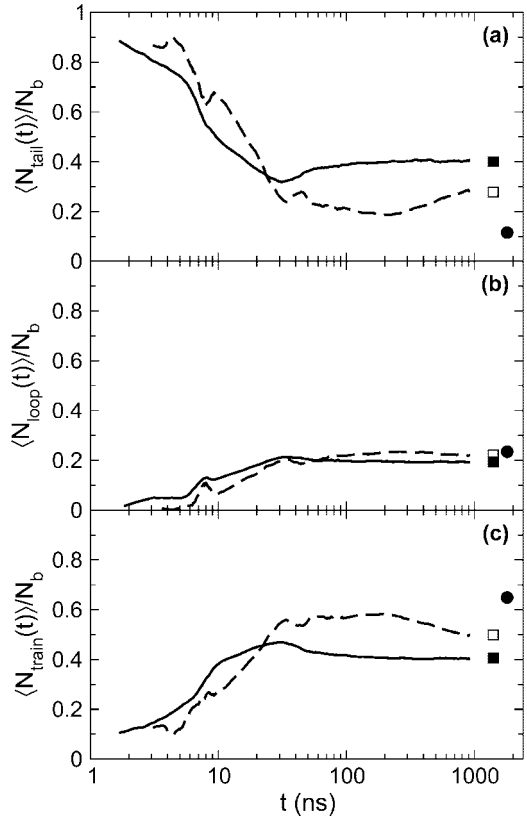

Figure 9. Average fraction of beads in (a) loops, (b) tails, and (c) trains $\langle N_\alpha(t)/N_b\rangle$, $\alpha = \{\text{loop, tail, train}\}$, for adsorbed polymers as a function of time t for the ld20 (dashed curves) and hd20 (solid curves) systems. Moving averages have been applied to reduce the noise level. The uncertainty is large at small t and negligible at large t. Corresponding equilibrium data obtained from MC simulations for the ld20 (open squares) and hd20 (filled squares) systems and for a single adsorbed polymer (filled circles) are also given.

values of the hd20 system appear $t \approx 30$ ns, and no significant variation of the tail, loop, and train characteristics appear after $t \approx 200$ ns, in agreement with previous finding. At the adsorption of a *single* and flexible 40-mer at otherwise identical conditions,[24] it was found that $\langle N_\alpha(t)/N_b\rangle$, $\alpha = \{\text{loop, tail, train}\}$, possessed *monotonic* relaxation to their equilibrium values. Furthermore, conformational equilibrium was attained ≈20 ns after attachment.

The appearance of a slow conformational relaxation in the present system, which (i) opposes the initial one, (ii) operates on the time scale of the relaxation of $N_p^{ads}(t)$, and (iii) is absent in a single-chain system, strongly indicates that this slow conformational relaxation involves a response of adsorbed polymers on the increasing number of adsorbed polymers. In particular for the ld20 system, the conformational relaxation occurring on a time scale of ≈10 ns is much faster than the relaxation of the number of adsorbed polymers having the time scale ≈1000 ns. Also in the hd20, the conformational relaxation appears faster than the relaxation of the number of adsorbed polymers.

Furthermore, $\langle N_b^{ads}(t)\rangle$ (could be obtained as $\langle N_p^{ads}(t)\rangle\langle N_{train}(t)\rangle$; remember that $\langle N_{train}(t)\rangle$ denotes the average number of trains of adsorbed polymers) displays a monotonic increase with t. The magnitude of the decrease of $\langle N_{train}(t)\rangle$ at large t is smaller than the increase in $\langle N_p^{ads}(t)\rangle$ at large t.

Finally, we notice that at equilibrium the fraction of beads in tails is larger, in loops is smaller, and in trains is smaller in the ld20 system as compared to the single-chain system, and furthermore, these trends continue as the solution density is increased. These observations are attributed to the progressively smaller surface area per chain, as deduced from the $\langle R_g^2\rangle_\parallel^{1/2}$ data given in Table 4.

In summary: (i) Numerous comparison of BD and MC results have shown that the ld20 system is close to become equilibrated at $t = 1000$ ns, which is the end of the BD simulation, whereas the denser hd20 system becomes equilibrated after $t \approx 200$ ns. (ii) The relaxation to the final equilibrium states of the $N_b = 20$ system is rather determined by the slow relaxation of the number of adsorbed polymers than the conformational relaxation of adsorbed polymers (Figure 9). (iii) The initial spreading of adsorbed polymers on the surface is partly reversed at the end of the equilibration process (Figures 8 and 9) due to excluded-volume interaction with other adsorbed polymers. Such a reversal has been predicted by Hasegawa and Doi from dynamic mean-field adsorption theory.[10] (iv) Finally, the larger adsorbed amount in the hd20 system leads to a stronger excluded-volume

interaction between beads residing in different coils, resulting in a larger perpendicular and smaller in-plane extension with a concomitant larger fraction of beads in tails and a smaller fraction of beads in loops and trains.

7. Discussion

Though the length of the polymers in the present simulation study is shorter, hence making the dynamics faster as compared to experimental systems, we believe that the observed general features should be of relevance, given that other conditions are held. In particular, Fu and Santore have examined the time-evolution of the adsorption of poly(ethylene oxide) onto silica in a flow-cell setup.[31] By combining Brewster angle reflectivity and total internal reflectance fluorescence (TIRF), along with the assumption of a single block layer with time-variable thickness and density, they concluded that the adsorbed layer evolves from a flat layer with a high density to a more extended one with lower density as the adsorbed amount reaches its equilibrium value. By a less ambitious analysis of cationic polyelectrolyte adsorption onto gold,[32] Claesson and co-workers deduced from a quartz crystal microbalance with built-in dissipation measurements that low-charged polyelectrolytes initially adsorb in a dense and flat structure, which then becomes less dense but more extended at longer times. Bearing in mind that a number of conditions differ among the experimental setups and our model simulations (initial states, polymer length, solvent condition, adsorption strength, etc.), we find a gratifying coherence: an initially flatter and denser adsorbed layer that becomes thicker and less dense as the adsorption process progresses.

8. Conclusions

Adsorption of flexible polymers from a bulk solution onto a planar surface has been examined by using Brownian dynamics. Start configurations consisting of equilibrated bulk solutions extended with 20 Å thick polymer-free slabs adjacent to two attractive surfaces were used. Hence, the full adsorption process including the diffusion of polymers to the surfaces was simulated. The number of adsorbed polymers and the bead density profiles were analyzed as a function of time. Furthermore, the frequency of exchange from adsorbed to nonadsorbed states was examined. Finally, the extensions of the polymer coils perpendicular and parallel to the surface as well as some conformational characteristics of adsorbed polymers were also investigated. Throughout, Monte Carlo simulation data were used to assess corresponding equilibrium properties.

Three systems have been considered, polymers with 20 and 80 beads, the former at two different polymer densities. In general, the adsorption process became faster for shorter polymers and at higher polymer density. The system comprising 20-mers at the high density became fully equilibrated after $\approx$1/5 of the simulation, whereas the two remaining systems came close but not fully to their equilibrium states.

As found for the adsorption of a single polymer, the adsorption process passes through several sequential steps, such as diffusion to the surface, anchoring onto the surface, and spreading on the surface. In addition, we found an additional process involving a shape and conformational readjustment of adsorbed polymers. This additional process appeared on the same time scale as the final relaxation of the number of adsorbed chains. Hence, we concluded that the slowest dynamics observed is the relaxation of the number of adsorbed polymers.

The equilibrium bead density profiles obtained by MC displayed one prominent maximum at the surfaces, a weaker second maximum, and a long-range tail. During the adsorption process, the buildup of the bead layer adjacent to the surfaces appears first, thereafter the second layer, and finally the long-range tail. Final equilibrium structures were only completely obtained for the high-density system with the shorter polymer length ($N_b = 20$) during the BD simulations.

Acknowledgment. The authors thank Håkan Wennerström for helpful discussions and the Center for Scientific and Technical Computing at Lund University (LUNARC) for generous allocation of computer resources. Financial support by the Swedish Research Council (VR) is also gratefully acknowledged.

References and Notes

(1) Fleer, G. J.; Lyklema, J. In *Adsorption From Solution at the Solid/Liquid Interface*; Academic Press: New York, 1983.
(2) Evans, D. F.; Wennerström, H. *The Colloidal Domain: Where Physics, Chemistry, Biology and Technology Meet*, 2nd ed.; Wiley-VCH: New York, 1999.
(3) Norde, W. *Colloids and Interfaces in Life Sciences*; Marcel Dekker: New York, 2003.
(4) Gray, J. J. *Curr. Opin. Struct. Biol.* **2004**, *14*, 110.
(5) Fleer, G. J.; Cohen Stuart, M. A.; Scheutjens, J. H. M. H.; Cosgrove, T.; Vincent, B. *Polymers at Interfaces*; Chapman & Hall: London, 1993.
(6) O'Shaughnessy, B.; Vavylonis, D. *J. Phys.: Condens. Matter* **2005**, *17*, R63.
(7) Scheutjens, J. M. H. M.; Fleer, G. J. *J. Phys. Chem.* **1980**, *84*, 178.
(8) de Gennes, P. G. *Macromolecules* **1981**, *14*, 1637.
(9) Douglas, J. F.; Johnson, H. E.; Granick, S. *Science* **1993**, *262*, 2010.
(10) Hasegawa, R.; Doi, M. *Macromolecules* **1997**, *30*, 3086.
(11) Striolo, A.; Prausnitz, J. M. *J. Chem. Phys.* **2001**, *114*, 8565.
(12) Wang, Y.; Rajagopalan, R. *J. Chem. Phys.* **1996**, *105*, 696.
(13) Xia, T. K.; Landman, U. *Science* **1993**, *261*, 1310.
(14) Zajac, R.; Chakrabarti, A. *J. Chem. Phys.* **1996**, *104*, 2418.
(15) Jia, L.-C. R.; Lai, P. Y. *J. Chem. Phys.* **1996**, *105*, 11319.
(16) Cohen Stuart, M. A.; Hoogendam, C. W.; de Kaiser, A. *J. Phys.: Condens. Matter* **1997**, *9*, 7767.
(17) Jan-Michael, Y. C.; Dobrynin, A. V. *Langmuir* **2007**, *23*, 2472.
(18) Pandey, R. B.; Milchev, A.; Binder, K. *Macromolecules* **1997**, *30*, 1194.
(19) Wolterink, J. K.; Barkema, G. T.; Cohen Stuart, M. A. *Macromolecules* **2005**, *38*, 2009.
(20) Takeuchi, H. *Macromol. Theory Simul.* **1999**, *8*, 391.
(21) Wang, Y.; Rajagopalan, R.; Mattice, W. L. *Phys. Rev. Lett.* **1995**, *74*, 2503.
(22) Wolterink, J. K.; Cohen Stuart, M. A.; Barkema, G. T. *Mol. Phys.* **2005**, *38*, 2009.
(23) Li, Y.; Wei, D.; Han, C. C.; Liao, Q. *J. Chem. Phys.* **2007**, *126*, 204907-1.
(24) Kallrot, N.; Linse, P. *Macromolecules* **2007**, *40*, 4669.
(25) Baschnagel, J.; Mayer, H.; Varnik, F.; Metzger, S.; Aichele, M.; Müller, M.; Binder, K. *Interface Science* **2003**, *11*, 159.
(26) Ermak, D. L.; McCammon, J. A. *J. Chem. Phys.* **1978**, *69*, 1352.
(27) Allen, M. P.; Tildesley, D. J. *Computer Simulations of Liquids*; Oxford University Press: Oxford, England, 1987.
(28) Linse, P. MOLSIM, Version 4.0, Lund University, Sweden, 2004.
(29) Le Guillou, J. C.; Zinn-Justin, J. *Phys. Rev. Lett.* **1977**, *39*, 95.
(30) Ponomarev, A. L.; Sewell, T. D.; Durning, C. J. *Macromolecules* **2000**, *33*, 2662.
(31) Fu, Z.; Santore, M. *Langmuir* **1997**, *13*, 5779.
(32) Plunket, M. A.; Claesson, P. M.; Ernstsson, M.; Rutland, M. W. *Langmuir* **2003**, *19*, 4673.

MA900050A